the plant journal

SEB SOCIETY FOR EXPERIMENTAL BIOLOGY

The Plant Journal (2023) **116,** 1529–1544 doi: 10.1111/tpj.16435

RESOURCE

Engineering of substrate specificity in a plant cell-wall modifying enzyme through alterations of carboxyl-terminal amino acid residues

Barbora Stratilová[1], Sergej Šesták[1], Eva Stratilová[1], Kristína Vadinová[1], Stanislav Kozmon[1,*] and Maria Hrmova[2,3,*]

[1]*Institute of Chemistry, Slovak Academy of Sciences, SK-84538 Bratislava, Slovakia,*

[2]*School of Agriculture, Food and Wine & Waite Research Institute, University of Adelaide, Waite Research Precinct, Glen Osmond, South Australia 5064, Australia, and*

[3]*Jiangsu Collaborative Innovation Centre for Regional Modern Agriculture and Environmental Protection, School of Life Science, Huaiyin Normal University, Huai'an 223300, China*

Received 17 May 2023; revised 7 August 2023; accepted 12 August 2023; published online 2 September 2023.
*For correspondence (e-mail maria.hrmova@adelaide.edu.au; stanislav.kozmon@savba.sk)

SUMMARY

Structural determinants of substrate recognition remain inadequately defined in broad specific cell-wall modifying enzymes, termed xyloglucan xyloglucosyl transferases (XETs). Here, we investigate the *Tropaeolum majus* seed TmXET6.3 isoform, a member of the GH16_20 subfamily of the GH16 network. This enzyme recognises xyloglucan (XG)-derived donors and acceptors, and a wide spectrum of other chiefly saccharide substrates, although it lacks the activity with homogalacturonan (pectin) fragments. We focus on defining the functionality of carboxyl-terminal residues in TmXET6.3, which extend acceptor binding regions in the GH16_20 subfamily but are absent in the related GH16_21 subfamily. Site-directed mutagenesis using double to quintuple mutants in the carboxyl-terminal region – substitutions emulated on barley XETs recognising the XG/penta-galacturonide acceptor substrate pair – demonstrated that this activity could be gained in TmXET6.3. We demonstrate the roles of semi-conserved Arg238 and Lys237 residues, introducing a net positive charge in the carboxyl-terminal region (which complements a negative charge of the acidic penta-galacturonide) for the transfer of xyloglucan fragments. Experimental data, supported by molecular modelling of TmXET6.3 with the XG oligosaccharide donor and penta-galacturonide acceptor substrates, indicated that they could be accommodated in the active site. Our findings support the conclusion on the significance of positively charged residues at the carboxyl terminus of TmXET6.3 and suggest that a broad specificity could be engineered *via* modifications of an acceptor binding site. The definition of substrate specificity in XETs should prove invaluable for defining the structure, dynamics, and function of plant cell walls, and their metabolism; these data could be applicable in various biotechnologies.

Keywords: computational chemistry, docking and molecular dynamics, donor and acceptor substrates, electrostatic potential, hetero-transglycosylation, pectin fragment, site-directed mutagenesis.

INTRODUCTION

Land plants classified in Embryophytes, which have evolved from Charophyta (green algae), possess characteristic polysaccharide-rich cell walls (CWs) (Cosgrove, 2005; Fry, 2004). CWs are multi-composite hydrogel structures that define the composition of their building blocks, and where variations in covalent and non-covalent linkages that adjoin polysaccharides, and their spatial distribution (Cosgrove, 2005, 2015; Farrokhi et al., 2009). Besides polysaccharides, another important constituent of CWs encompasses proteins (including non-catalytic expansins) and various inorganic and organic compounds, including non-fermentable hydrophobic phenylpropanoid lignin. Despite certain shared characteristics, the composition of CWs varies in plant species (Popper & Fry, 2003, 2004), organs, and tissues (Burton et al., 2010; Fangel et al., 2012; Fincher, 2009; Kozlova et al., 2020; Sørensen et al., 2010), during growth and developmental stages (Iraki et al., 1989),

adaptations to living environments, and biotic and abiotic (environmental) stresses (Kutsuno et al., 2023; Popper et al., 2011). The remarkable diversity of CWs underlies their multiple functions, which include mechanical support, diffusion of compounds, growth regulation, cell-to-cell communication (Popper et al., 2011), the definition of shape and size of a plant, formation of barriers to pathogens or resistance against turgor pressure and restrictions of the rate and direction of cell expansion (Fry et al., 2011). Other roles of CWs also include cell-to-cell adhesion in multicellular plant organisms, the sequestration of toxic metal ions, and the production of signalling compounds, such as oligosaccharins (Ochoa-Meza et al., 2021).

There are two types of CWs in plants [primary (PCWs) and secondary (SCWs)], where these dynamic PCWs, composed of networks of cellulose microfibrils tethered by cross-linking glycans (Scheller & Ulvskov, 2010), are present mostly in di-cotyledonous plants. Here, cellulose microfibrils are interconnected by variously substituted xyloglucans (XGs), while in mono-cotyledonous and lower plants these linking is mediated by xylans (arabinoxylan and glucuronoarabinoxylan), mannans (galactomanan, glucomannan, and galactoglucomannan), and (1,3;1,4)-β-D-glucans (Fry, 2004; McCann & Knox, 2011). In most dicotyledonous plants these polysaccharides are embedded in the matrix of pectins (Marcus et al., 2008; Popper & Fry, 2005), other glycans, and glycoproteins. Conversely, SCWs are typical of woody and vascular plants after they cease growing, contain less pectin, more cross-linking glycans, and are reinforced by lignin (Boerjan et al., 2003; Mnich et al., 2020; Weng & Chapple, 2010) to ensure roles in the mechanical stability of woody plants (Déjardin et al., 2010; Kushwah et al., 2020).

In Embryophytes, XGs consist of repeating (1,4)-β-D-linked glucopyranosyl moieties such as cellulose, but with C-6 carbons carrying α-D-xylopyranosyl residues which could be substituted by galactopyranosyl residues on C-2 carbons. Galactosyl moieties could carry the fucopyranosyl branchings (Hayashi, 1989; York et al., 1990), and in moss and liverwort XGs, arabinopyranosyl and galacturonate substituents are present instead of the fucopyranosyl residues (Peña et al., 2008). Although, notably, galacturonic acid-containing XGs were found in *Arabidopsis thaliana* root hair tips (Peña et al., 2012). The backbone of glucopyranosyl and side chain galactopyranosyl residues could be acetylated (Pauly & Keegstra, 2016). The XG backbones are synthesised by an XG:glucan synthase encoded by the members of the C-subfamily of cellulose synthase-like (*CSL*) genes (Cocuron et al., 2007; Kim et al., 2020), but only when both UDP-glucose and UDP-xylose are present, implying that the presence of another enzyme, XG:xylosyltransferase, is obligatory to synthesise XGs (Cavalier et al., 2008; Cavalier & Keegstra, 2006; Culbertson et al., 2016; Faik et al., 2002; Vuttipongchaikij et al., 2012; Zabotina et al., 2008, 2012). Further substitutions are mediated by XG:galactosyltransferases (Jensen et al., 2012; Madson et al., 2003), XG:fucosyltransferases (Perrin et al., 1999; Vanzin et al., 2002), and acetylation of XGs is conducted by acetyltransferases (Gille et al., 2011; Liu et al., 2016; Zhong et al., 2017, 2018, 2020).

As life processes in plants are guided by CWs and their organisations/re-organisation processes, the modifications of cross-linking XGs (and other structural polysaccharides) are thought to be one of the key processes during CW elongation, expansion, and loosening (Franková & Fry, 2013; Thompson et al., 1997). This could occur through *in situ* cleavage of XG linkages, incorporation of new components, or re-construction of polymers through cross-linking mediated by hydrolysis or transglycosylation reactions. For XGs, these processes are moderated by hydrolases/transglycosylases of the GH16_20 subfamily (Eklöf & Brumer, 2010; Viborg et al., 2019). Members of the GH16_20 subfamily exhibit either xyloglucan endo-transglycosylase (XET, EC 2.4.1.207) or xyloglucan endo-hydrolase (XEH, EC 3.2.1.151) activities (Baumann et al., 2007; Kaewthai et al., 2013), where XET and XEH enzymes, often labelled as XTHs, play key roles in plant growth (Eklöf & Brumer, 2010; Rose et al., 2002).

The fundamental feature of catalytic mechanisms of XETs and XEHs is the binding of the XG molecule (donor substrate) and breaking (1,4)-β-glycosidic linkages of the polysaccharide backbone during the first step of a reaction, while in the second step, XETs transfer an XG-fragment with an original non-reducing terminal onto a saccharide acceptor, while XEHs use an activated water molecule as an acceptor (Drula et al., 2022; Hrmova et al., 1998). Both types of reactions follow the so-called ping-pong bi-bi mechanism (Baran et al., 2000; Saura-Valls et al., 2006), which proceeds in two stages that incorporate two transition states (Johansson et al., 2004). The first step involves the deprotonation of a nucleophile (Glu amino acid residue), which attacks the anomeric carbon of a scissile glycosidic linkage adjoining glucose moieties, while another Glu acts as an acid/base, which deprotonates a glycoside acceptor; the third Asp residue controls the protonation states of both Glu residues (Drula et al., 2022; Johansson et al., 2004). The preference for a transfer reaction, instead of a hydrolytic one by XETs, leads to the re-ligation of the nascent donor end of a saccharide moiety at the non-reducing terminal of an acceptor substrate (Johansson et al., 2004; Mark et al., 2009).

The structure of the GH16_20 subfamily XETs is represented by poplar PttXET16A (Protein Data Bank - PDB 1un1 or 1umz, Johansson et al., 2004) that adopts a β-jelly-roll topology and folds into two antiparallel β-sheets, which form the β-sandwich consisting of convex and concave regions. The catalytic machinery is located in the middle of the convex region and has either the EXDXXE motif in

subgroup I (GH16_1 to GH16_17 subfamilies) or an EXDXE motif in subgroup II (GH16_18 to GH16_23 subfamilies) (Viborg et al., 2019). In comparison to other GH16 subfamilies, the GH16_20 members encompass a carboxyl-terminal region located near the convex part of the structures (residues 208–272 in PttXET16A), that form two α-helices, and another β-strand with associated loops, on a concave side of a molecule. This addition extends the active site for the binding of acceptor substrates (Viborg et al., 2019). Another characteristic feature of this subfamily is the presence of a well-conserved loop region (residues 181–190) positioned near a catalytic site with strictly conserved Trp195 forming a hydrophobic platform at the +1 subsite, the occurrence of short loops bordering the active-site cleft at negative subsites (Johansson et al., 2004), and another aromatic platform formed by Tyr81 rather than tryptophan residue at the −1 subsite, which is observed in other GH16 members (Viborg et al., 2019). The broadening of the active-site cleft, resulting from the loop shortening located at negative subsites, is thought to be responsible for the recognition of a branched XG chain (Eklöf et al., 2013; McGregor et al., 2017). Major differences between PttXET16A and TmNXG1 (XEH, PDB 2uwa; Baumann et al., 2007), are in three loops that extend the active-site cleft at positive subsites, which assure the binding of acceptor substrates. The importance of one of these loops was verified in the TmNXG1-DYNIIG mutant (PDB 2vh9; Mark et al., 2009), in which loop substitutions led to a sixfold lowering of hydrolytic and a twofold increase of the transglycosylation activities, relative to those in wild-type (WT) TmNXG1. In concert with the active-site loop changes, the fine-tuning of substrate interactive forces (through subtle variations of hydrogen bond and hydrophobic interactions, which are crucial noncovalent forces shaping and maintaining protein structures), modulates a fine ratio between hydrolytic and transglycosylation activities (Mark et al., 2009).

Notable substrate specificity differences in XET mutants were observed, where protein sequence alterations were introduced near their active sites (Hrmova et al., 2007; Stratilová et al., 2019, 2020). In further studies, using the hetero-trans-β-glucanase (HTG) from *Equisetum*, the increased activity with the cellulose donor substrate was attributed to mutations at positions 10 and 34, where tryptophan and glycine residues were replaced by those of proline and serine, respectively; the latter residues directly participated in donor binding (Holland et al., 2020; Simmons et al., 2015). The validity of data, supported by molecular modelling of HvXET5 (Hrmova et al., 2007) and AtXTH3 (Shinohara et al., 2017), which exhibit high catalytic rates with the cellulose donor, pointed to equivalent positions of proline and serine residues.

Further, it was reported that most XETs contain Q102/R116 (PttXET16A) or the corresponding H94/Q108 (TmXET6.3) residue combinations (Shinohara & Nishitani, 2021). But unlike the Q102/R116 residues (which are adjacent to catalytic nucleophile E89) in XG-specific PtXET16A (Johansson et al., 2004), the analyses of non-specific TmXET6.3 showed, that the H94/Q108 pair was essential for interactions with a wide spectrum of structurally distinct neutral acceptors (Hrmova et al., 2022; Stratilová et al., 2019, 2022).

Further differences were observed through molecular modelling of TmXET6.3 and comparison with non-specific HvXET3, HvXET4, and HvXET6, which in addition to neutral acceptors, catalysed XG or hydroxyethyl cellulose (HEC) transfers to a negatively charged (acidic) pentagalacturonide pectin fragment $[\alpha(1\text{-}4)\text{GalA}p]_5$ (Stratilová et al., 2020). In HvXETs, the residues in positions 75 and 110 were responsible for these activities, which was confirmed by the W75H and Y110R mutations in TmXET6.3, creating W75H/Y110R that recognised the XG/$[\alpha(1\text{-}4)\text{GalA}p]_5$ substrate pair (Stratilová et al., 2020).

It was also reported that the R246L mutation in HTGs can be responsible for increased activity with the cello-oligosaccharide (Cello-OS) acceptor (Holland et al., 2020), however, this has yet to be verified because TmXET6.3 (Stratilová et al., 2019), *Equisetum* XTHs (Holland et al., 2020), and HvXET3, HvXET4, and HvXET6 (Stratilová et al., 2020), which also catalyse transfer with Cello-OS, have an arginine residue in equivalent positions, while AtXTH3 (Shinohara et al., 2017) has the lysine residue. Similar results, *i.e.* activity increases with Cello-OS were obtained with the K234T/K237T mutant of TmXET6.3 (Stratilová et al., 2019) – the K237 residue localises to the vicinity of conserved R258, which corresponds to L246 in HTGs (Holland et al., 2020). All residues located at the carboxyl terminus of XETs, extend an acceptor binding site, which is prototypical of the GH16_20 subfamily, and thus, could interact with acceptors.

The structural differences modulating donor and acceptor substrate binding are reflected in phylogenetic relationships of the GH16 family, spanning monocots, eudicots, and a basal Angiosperm (Stratilová et al., 2020). Here, in the Randomised Axelerated Maximum Likelihood tree of 419 GH16 sequences, constructed using the maximum likelihood phylogenetic reconstruction method, XETs of the GH16_20 subfamily (Viborg et al., 2019) created various lineages reflecting their substrate specificity. Based on these and other analyses, it was postulated that the evolution of broad specific XETs (Stratilová et al., 2020) could have progressed through multiple gene duplication (Behar et al., 2018) and neo-functionalisation to secure their biological roles (Akdemir et al., 2022; Seven et al., 2021; Shinohara & Nishitani, 2021; Stratilová et al., 2020; Viborg et al., 2019). Noteworthy, *XTH* (both *XET* and *XEH*) genes are not present in all plants or algae but are present in algae closely related to land plants (Eklöf & Brumer, 2010). It was postulated that XEHs could have evolved through a

gain of function of ancestral GH16 from XETs by a simple loop extension (Baumann et al., 2007), additions of two-three, or more residues (McGregor et al., 2017), and co-evolution of substrate-binding residues (Shinohara & Nishitani, 2021) to broaden their active site clefts (McGregor et al., 2017). Nonetheless, despite signature definitions of XET and XEH enzymes, the exhaustive understanding of their evolution requires further considerations.

We have previously observed that TmXET6.3 exhibits high positional sequence identity/similarity with barley HvXET3 (57/74%), HvXET4 (55/72%), and HvXET6 (59/74%) isoforms, and that TmXET6.3 clusters in the same lineage as HvXET6, and neighbours the lineage of HvXET3 and HvXET4 (*cf.* Figure 7, Stratilová et al., 2020 therein). Based on these findings and our previous investigations (Stratilová et al., 2019, 2020), in this work, we perform additional mutational and structural bioinformatics study of TmXET6.3. This study is grounded on similarities to the carboxyl-terminally located positively charged residues, specifically those of lysine residues confined near conserved Arg238 in TmXET6.3, and in HvXETs (as specified above), which underlie the recognition of negatively charged $[\alpha(1\text{-}4)\text{GalA}p]_5$. We complement these data by defining molecular interactions in individual XG/$[\alpha(1\text{-}4)\text{GalA}p]_5$ complexes of WT and mutant TmXET6.3, and compare them with those of selected barley HvXETs. We discuss the significance of the broadened heterotransglycosylation activity of TmXET6.3 in the structure, dynamics, and function of plant CWs and metabolism.

RESULTS AND DISCUSSION

Enzymes in the GH16 network represent a large and taxonomically diverse group of hydrolases and transferases, with a unifying feature of their β-jelly-roll topology. These enzymes are classified into 23 subfamilies (Viborg et al., 2019), where explicitly the GH16_20 subfamily contains the enzymes with XET (EC 2.4.1.207) and XEH (EC 3.2.1.151) activities (http://www.cazy.org/GH16_20_structure.html). On the other hand, the GH16_21 subfamily (http://www.cazy.org/GH16_21_structure.html) includes hydrolases (with licheninase or lichenase activities; EC 3.2.1.73), which participate in the hydrolysis of (1,3;1,4)-β-D-glucans (Keitel et al., 1993).

It has previously been postulated that residues localised at the carboxyl termini of the XET GH16_20 subfamily extend their acceptor binding sites (Eklöf & Brumer, 2010; Hrmova et al., 2009; Viborg et al., 2019), compared to *e.g.* GH16_21 licheninases, which embody one of the shortest sequences in the GH16 family. This carboxyl-terminal extension of around 60 residues (DAFQYRRLSWVRQKYTIYNYCTDRSRYPSMPPECKRDRD) (Figure 1a) in PttXET16A has unique structural attributes, as confirmed by PDB archive search (https://www.rcsb.org/search/advanced/structure) of structural similarity. In XETs, this carboxyl-terminal extension serves as part of an acceptor binding site, mediating key interactions with acceptor substrates (Figure 1b). Here, the broadening of the active-site cleft, resulting from the loop shortening at negative subsite binding sites, is thought to be responsible for the recognition of branched XG chains (Eklöf et al., 2013; McGregor et al., 2017). As for the comparisons between XETs and XEHs, one exception includes a loop that precedes the strand containing the catalytic EXDXE motif, which is specifically lengthened in XEHs (Baumann et al., 2007).

In our previous work (Stratilová et al., 2019) we observed, that in non-specific nasturtium TmXET6.3, the H94, and Q108 residues, and in PttXET16A the Q102 and R116 residues, that locate spatially close to active sites, are essential for mediating interactions with a narrow (PttXET16A) or broad (TmXET6.3) spectrum of neutral acceptor substrates (Hrmova et al., 2022; Stratilová et al., 2019, 2022). This is supported by the visualisation of the molecular dynamics (MD) trajectory of the XXXG/neutral manno-tetra-oligosaccharide substrate pair in WT TmXET6.3 (broad specific) and PttXET16A (specific) (Video S1). These snapshots point out that TmXET6.3 retains both substrates in the active site, which could eventuate in covalent bond formation (Stratilová et al., 2019), while PttXET16A is unable to do so.

With the aim to clarify the impact of residues located at the carboxyl terminus of TmXET6.3 on its heterotransglycosylation activity with the charged acceptor $[\alpha(1\text{-}4)\text{GalA}p]_5$ substrate (a pectin fragment), we embarked on a mutational analysis using the XG donor and a series of acceptor substrates (Scheme S1). These investigations included conserved R238 – the mutation to alanine, K237 – mutations to threonine and tryptophan, and other residues, and converting neutral S240 and Q241 to the lysine residues, thus creating double to quintuple mutant combinations of these residues (Figure 1a).

As outlined, carboxyl-terminal regions of the GH16_20 subfamily of the GH16 network are extended, compared to the other subfamily enzymes of the GH16 group (Figure 1a,b). In Arabidopsis, azuki bean, poplar, nasturtium, and barley XETs, this extension covers between 55–67 residues (*cf.* Figure 3, Hrmova et al., 2009 therein), compared to a prototypical GH16_21 enzyme (1,3;1,4)-β-D-glucan 4-glucanohydrolase from *Bacillus licheniformis* (PDB 1 gbg; Hahn et al., 1995). At a structural level, this carboxyl-terminal extension in the GH16_20 subfamily corresponds to accompanying secondary structural elements that fold into two α-helices, one β-strand, and associated loops, as observed in the crystal structure of PttXET16A (Johansson et al., 2004) (Figure 1a,b).

To investigate the effects of mutations in the carboxyl-terminal region of TmXET6.3, we calculated and compared the surface charge distributions in barley, nasturtium, and poplar XETs (Figure 1c). Unlike strongly negative

(a)

```
Conservation:                                          9 96     66 996   69969969  9     6 99
GH 21          214  R-------------------------------------------------------------------------  214
PtXET16A       213  CEA-SVEAKFCAT----------QGARWWDQKEFQDLDAFQYRRLSWVRQKYTIYNYCTDRSRYPS-MPPECKRDRD-  277
HvXET5         207  CEA-SAEAKLCA-----------QGARWWDQPEFQDLDAAQYRRLAWVRKEHTIYNYCTDRERYAA-MSPECKRDRDV  271
HvXET6         201  CAS-QDAA---------------ACANSNGAWMYQELDATALDRLQWVQKNYMIYNYCTDTWRFKDGAPPECASK---  259
HvXET4         208  CVM-SGGAQRCPAGTME------ASAAGGGSWWNQELSGMGYRRMRWVQRKFMIYNYCTDPKRVAQGVPAECKLR---  275
HvXET3         202  CVVTAGGRPRCGASMGTEAAPGTGASGAAGEWYNQELDLTLQQRMRWVQSNYMIYNYCTDPKRVAKGVPAECSM----  275
TmXET6.3       199  NKN-PSTST----------------------WFSQQLDSNSKEKLKWVRDNYMIYDYCKDFKRFSQGLPRECSVN---  250
Consensus ss:                                      hhhhhhhhhhhhh  eee
```

(b)

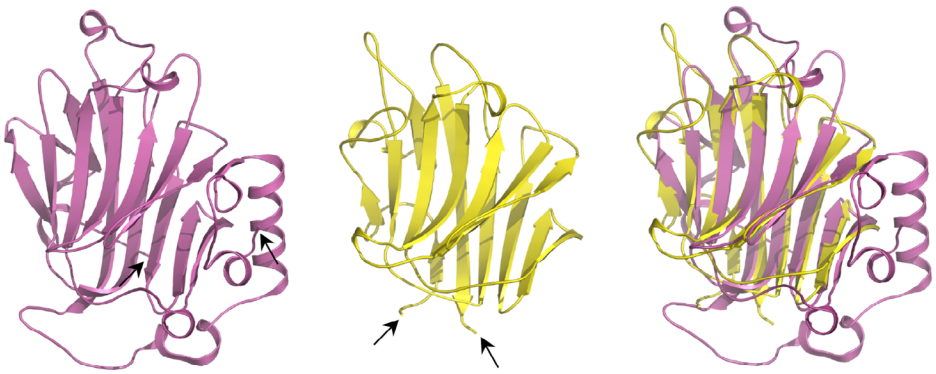

(c)

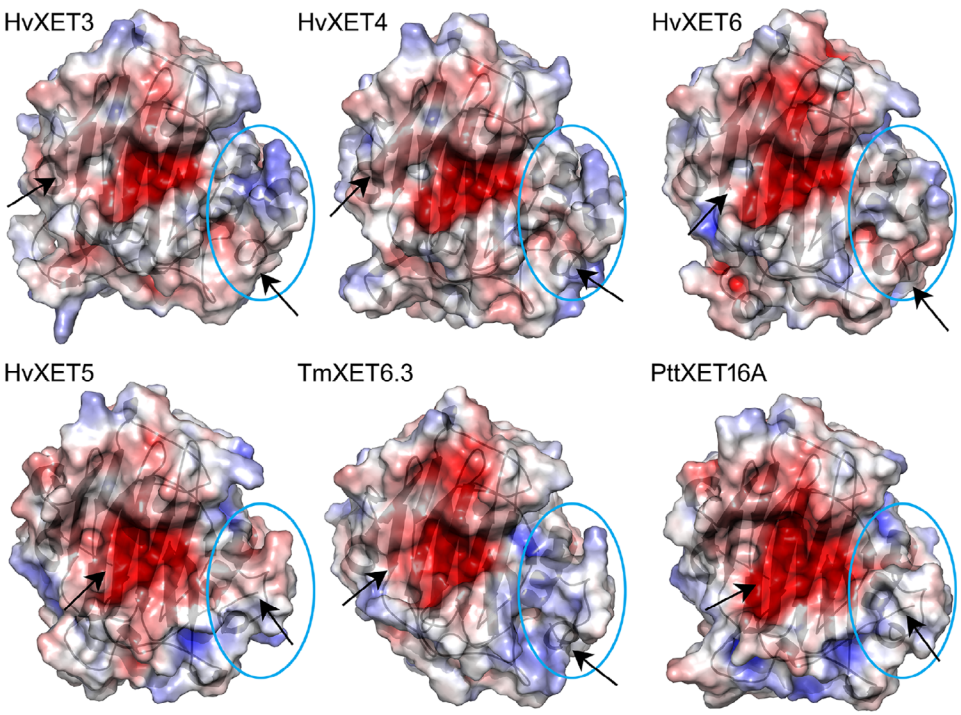

Figure 1. Structural characteristics of selected members of GH16_20 (XETs) and GH16_21 (licheninases) members.
(a) Alignment of carboxyl-terminal regions of GH16_20 (TmXET6.3, HvXET3 to HvXET6 and PtXET16A) and GH_21 (1,3;1,4)-β-D-glucan 4-glucanohydrolase; UniprotKB P27051) in ProMals3D (Pei et al., 2008) indicates the absence of a carboxyl-terminal region in GH_21 enzymes. Conservation indices shown on the top of the alignment are on a scale of 1–9. Grey boxes indicate residues subjected to mutagenesis in this study. Terms ss, h, and e indicate secondary structures, α-helix, and β-strands, respectively.
(b) Comparisons of tertiary folds of crystal structures GH16 family members (PttXET16A; GH16_20; PDB 1un1; magenta, left, and (1,3;1,4)-β-D-glucan 4-glucanohydrolase; GH16_21; PDB 1gbg; yellow, middle), and their superimpositions (right) with the RMSD value of 1.2 Å. NH_2^- and carboxyl termini in each structure are indicated by arrows.
(c) Surface morphologies of 3D models of HvXET3 to HvXET6, TmXET6.3, and the PttXET16A crystal structure are coloured by electrostatic potentials (white, neutral; blue, +5 kT e^{-1}; red, −5 kT e^{-1}). Carboxyl-terminal extensions (cyan ovals), and respective top and bottom arrows point to NH_2^- and carboxyl termini of each enzyme.

The Plant Journal published by Society for Experimental Biology and John Wiley & Sons Ltd.,
The Plant Journal, (2023), **116**, 1529–1544

electrostatic potentials around their catalytic sites, which are required to regulate protonation states of catalytic residues, the electrostatic potentials carried both negative and positive patch charges, where positive charges were most pronounced at the carboxyl termini of HvXET3 and TmXET6.3 (Figure 1c).

As referred to previously, the H94/Q108 residue combination in non-specific TmXET6.3 permits to catalyse transfers of XG or HEC fragments into a whole spectrum of structurally distinct neutral acceptors (Shinohara & Nishitani, 2021; Stratilová et al., 2019, 2022). This can be correlated with a positive charge distribution at carboxyl termini in TmXET6.3 or HvXET3, HvXET4, and HvXET6 (in HvXETs the values decrease in the given order) (Figure 1c). The importance of the H94/Q108 combination for the TmXET6.3 broad substrate specificity, compared to the Q102/R116 residue combination in PttXET16A (Shinohara & Nishitani, 2021), was confirmed by mutation analyses (Stratilová et al., 2019) and computational chemistry tools; the latter monitors the stability of enzyme-donor-acceptor complexes (Figure S1) (Stratilová et al., 2022). As reported, the HvXET3, HvXET4, and HvXET6 isoforms (Stratilová et al., 2020) transferred the XG or HEC fragments onto the charged penta-galacturonic acid acceptor [α(1-4)GalA*p*]$_5$ (Stratilová et al., 2020), with the activity decreasing in that order; Table 1). For TmXET6.3, which carries a positive charge at the extended acceptor binding site, two mutations W75H and Y110R were introduced, based on the analysis of HvXETs. These mutations were obligatory to increase the positive charge in the acceptor site (Figure S2) and supported the catalytic activity with [α(1-4)GalA*p*]$_5$ (Stratilová et al., 2020). On the other hand, specific HvXET5 and PttXET16A with the Q102/R116 residue combination (Shinohara & Nishitani, 2021) exhibited negative or slightly negative electrostatic potentials at the carboxyl-terminal regions (Figure 1c) and could not bind [α(1-4)GalA*p*]$_5$ (Table 1). However, these enzymes bound neutral acceptors with glucose moieties linked by (1,3)- and (1,4)-glycosidic linkages (Stratilová et al., 2022), although the activity with (1,4)-β-linked oligosaccharides was experimentally detected only in HvXET5 (Hrmova et al., 2007).

Most XETs contain an arginine residue in their carboxyl-terminal regions (*e.g.* R238 in TmXET6.3; Figure 1a). However, two other enzymes, *Equisetum* EfHTG and Arabidopsis AtXTH3 that exhibit increased activities with Cello-OS as acceptors, have leucine and lysine instead of an arginine residue in these positions (Shinohara et al., 2017; Simmons et al., 2015). To verify the assumption regarding the correlation between residue requirements in these positions and enzyme activities on structurally distinct acceptors (Holland et al., 2020), R238A mutation was introduced into TmXET6.3 and in the W75H/Y110R mutant, with the aim to assess the activity with a variety of acceptors (Figure 2a). The size-exclusion HPLC profile (where we monitor fluorescence increase due to the incorporation of SR-labelled acceptor substrates) of R238A indicates that fluorescence increased linearly in time with the XG/La-OS5 substrate pair (Figure 2b). Notably, the mutation of Arg238 increased the activity with the neutral Cello-OS and β(1–4,1-4,1-3)Glc*p*$_4$ acceptors by about 44% and 16%, respectively (Figure 2c). This mutation with bound XXXG led to a substantial increase in hydrogen bond separations between the catalytic residues (E77, D79

Table 1 Hetero-transglycosylation activities of the TmXET6.3 W75H/Y110R double mutant, barley HvXET3 to HvXET6 isoforms, and poplar PttXET16A with the XG/[α(1-4)GalA*p*]$_5$ substrate pair. The occurrence of basic amino acid residues in their C-terminal regions is indicated

Enzyme[a]	Activity[b]	K234[c]	K237[c]	R23[c]	K240[c]	K241[c]
TmXET6.3 W75H/Y110R	+++	K234	K237	R238	–	–
HvXET3 (P93671)	++(+)	–	K260	R261	–	K264
HvXET4 (P93672)	+(+)	–	K253	R254	–	–
HvXET6 (B1P1S7)	+	–	–	R247	K249	–
HvXET5 (P93668)	–	–	–	R258	–	–
PttXET16A (Q8GZD5)	–	–	–	R258	–	–

[a]UniprotKB accessions are specified.
[b]Activity is expressed as high (+++), medium [++(+) to +(+)], weak (+), and absent (–).
[c]Numbering of amino acid residues corresponds to that of TmXET6.3.

Figure 2. The R238A mutation in TmXET6.3 influences hetero-transglycosylation activity with the XG donor and structurally diverse oligosaccharide acceptors.
(a) Abbreviations, descriptions, and chemical structures of commercial and purified acceptor oligosaccharides used in this work. Chemical formulas are defined in Scheme S1.
(b) Right panel: Size-exclusion HPLC of the R238A reaction with the XG/La-OS5 substrate pair generating fluorescent products with average molecular masses of 60 to 100 kDa. Respective double and single arrows indicate XG with incorporated SR-labelled La-OS5 (retention time 11 min) and SR-labelled La-OS5 acceptor (retention time 22 min). Left panel: Time-dependent evolution of fluorescent XG product with La-OS5. The average data of three technical replicates (n = 3) are plotted with standard deviation values calculated via Excel in Microsoft Office Professional 2016.
(c) The relative activity to the XG/XG-OS8 substrate pair (100%) indicates activities of WT (white) and the R238A mutant (light grey) of TmXET6.3 with each acceptor. Standard deviations were calculated from three (n = 3) technical replicates.
(d) Respective right- and left-hand images with bound XXXG illustrate separations (dashed lines) between R238 (WT) or R238A and catalytic residues (cpk sticks and spheres).

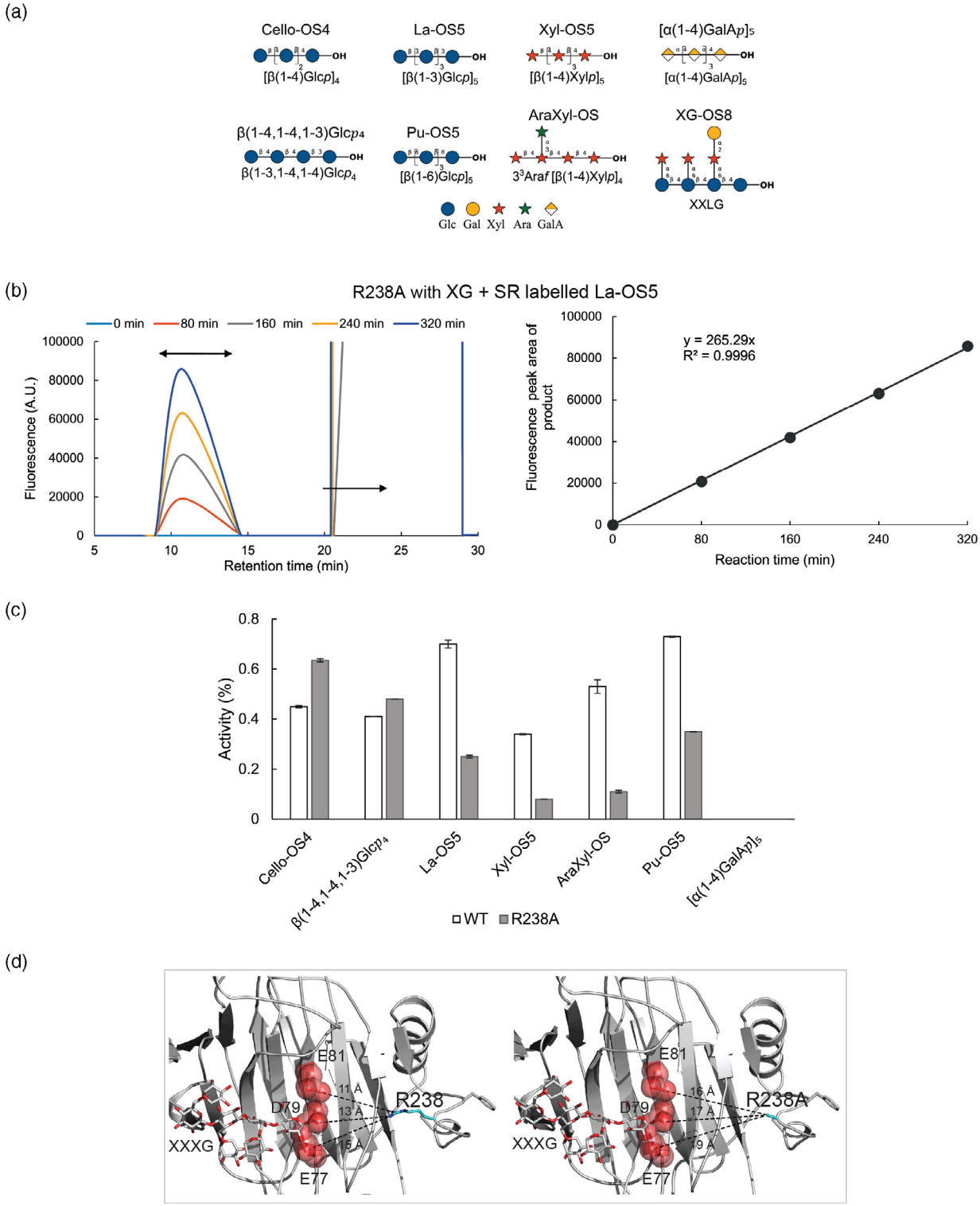

and E81) and R238A, compared to those in WT TmXET6.3 (Figure 2d). The increase of TmXET6.3 R238A activity with the XG/Cello-OS substrate pair was also observed with a double K234T/K237T mutant of residues that are adjacent to R238 (Stratilová et al., 2019). But, as reported, hetero-transglycosylation activities of other TmXET6.3 mutants were suppressed, including the double K234T/K237T mutant (Stratilová et al., 2019), while WT TmXET6.3 exhibited no activity with ionic acceptors such as [α(1-4)GalA*p*]$_5$ (Stratilová et al., 2020); as observed, the R238A mutation

could not change this outcome (Figure 2c). In summary, we showed with the R238A mutant, that the efficiency of transfers (compared to WT) to XG with neutral acceptors could be higher [Cello-OS4 and β(1–4,1-4,1-3) Glcp4] or lower (La-OS5, Xyl-OS5, AraXyl-OS, Pu-OS5) (Figure 2c). This was also reported previously (Stratilová et al., 2019), where the TmXET6.3 mutant altered in K234 and K237 at its carboxyl terminus showed increased activity with Cello-OS.

As outlined above, the differences in electrostatic charge distribution of the carboxyl-terminal regions in XETs (residues 234–241; Figure 1a) could be attributed to the presence of lysine residues (Figure 3). To confirm this observation, further mutations were introduced in the double W75H/Y110R mutant of TmXET6.3, which reflected the changes in the distribution of electrostatic potentials (Figure S2). These additional mutations (generating triple to quintuple TmXET6.3 mutants) reflected the equivalent positions of lysine residues in HvXET3 (W75H/Y110R/K234T, W75H/Y110R/Q241K, W75H/Y110R/K234T/Q241K), HvXET4 (W75H/Y110R/K234T) and HvXET6 (W75H/Y110R/K234T, W75H/Y110R/K237W, W75H/Y110R/S240K, W75H/Y110R/K234T/K237W, W75H/Y110R/K234T/Q241K and W75H/Y110R/K234T/K237W/S240K). The size-exclusion HPLC profiles indicate that the observed fluorescence intensities (or fluorescence signals) increased with W75H/Y110R, W75H/Y110R/S240K and W75H/Y110R/K234T/K237W linearly in time with the XG/[α(1-4)GalA*p*]$_5$ substrate pair – the most pronounced increase was seen with W75H/Y110R/S240K (Figure 4a). Upon additionally adding K234T and K237W mutations in W75H/Y110R, we observed an approximate 91% decrease in activity with ionic acceptors, compared to W75H/Y110R (Figure 4b). This occurred due to a loss of at least one basic residue, which likely stabilised the negatively charged acceptor in the TmXET6.3 acceptor binding site and reflected substrate-enzyme charge matching. Conversely, the replacements of neutral S240 or Q241 with lysine residues in W75H/Y110R increased the hetero-transglycosylation activity above the activity of W75H/Y110R (Figure 4b). Compared to the double W75H/Y110R mutant, the increased hetero-transglycosylation activities with the XG/[α(1-4)GalA*p*]$_5$ substrate pair were only observed for the W75H/Y110R/S240K and W75H/Y110R/Q241K mutants (Figure 4b). These

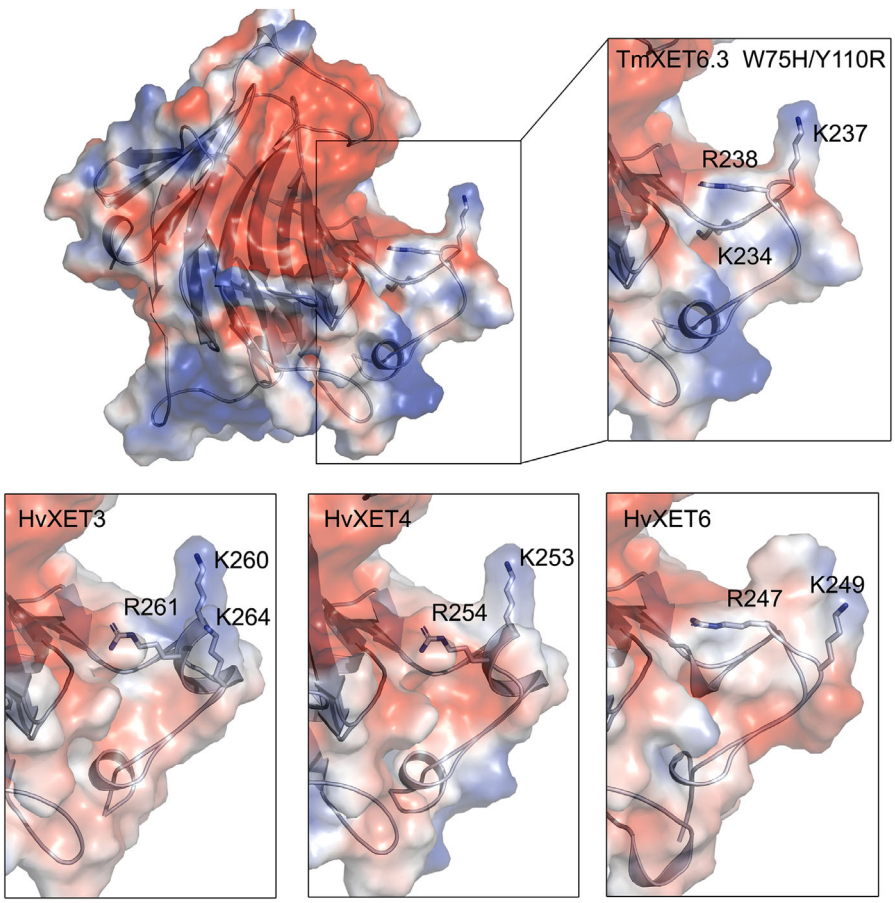

Figure 3. Dispositions of basic lysine and arginine residues in carboxyl-terminal regions of molecular models of TmXET6.3 W75H/Y110R, and HvXET3, HvXET4 and HvXET6 that support transfer reactions with XG or HEC and negatively charged [α(1-4)GalA*p*]$_5$ acceptor substrate pairs.

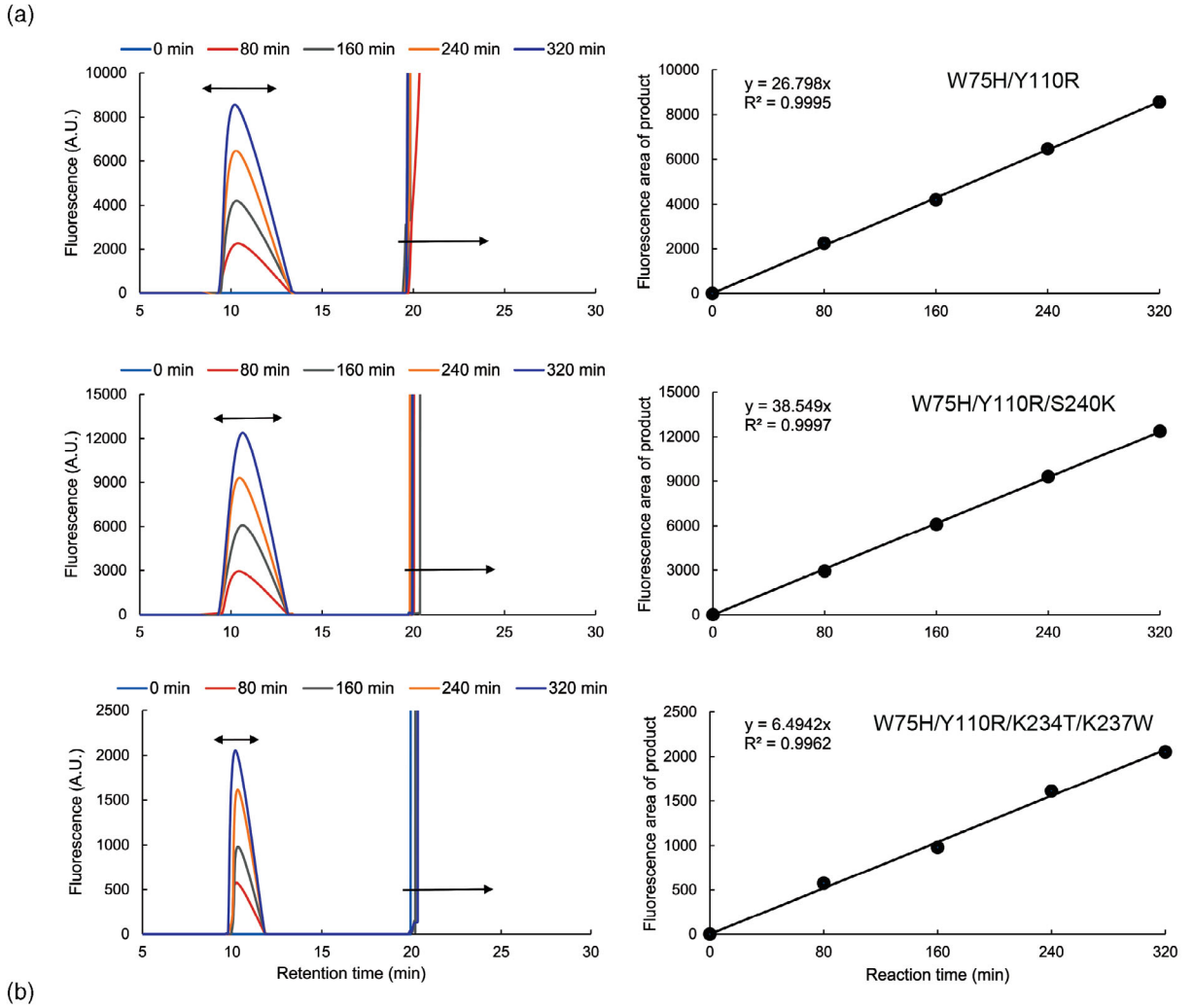

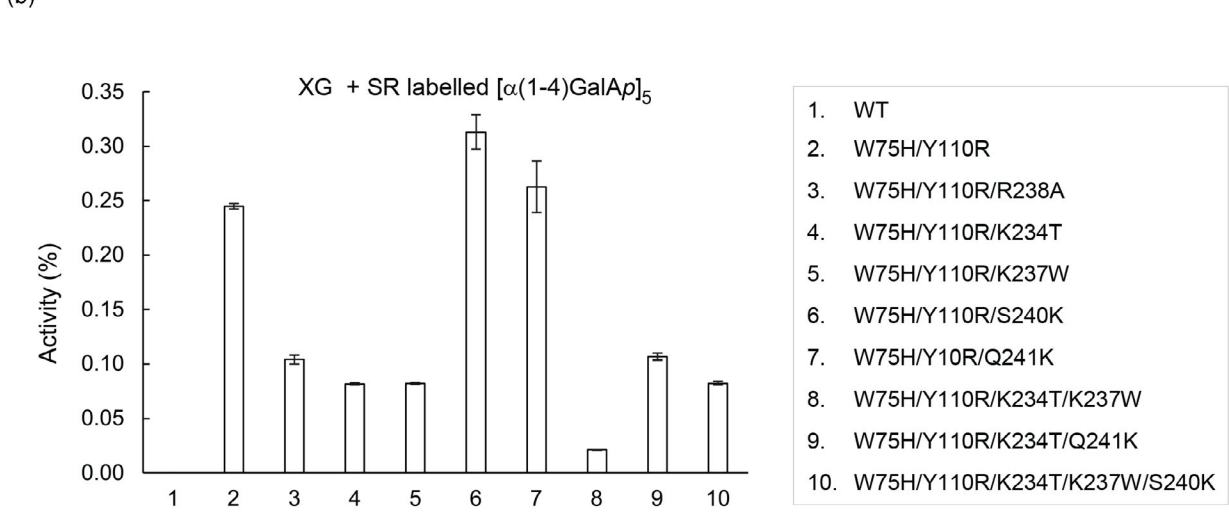

Figure 4. Hetero-transglycosylation activities of double to quintuple TmXET6.3 mutants, and HvXET3, HvXET4, and HvXET6 isoforms with the XG/[α(1-4)GalA*p*]$_5$ substrate pair.
(a) Right and left panels: Size-exclusion HPLC of W75H/Y110R (top) W75H/Y110R/S240K (middle) and W75H/Y110R/K234T/K237W (bottom) with the XG/[α(1-4)GalA*p*]$_5$ substrate pair generating fluorescent products with average molecular masses of 60–100 kDa, as described in Figure 2, panel b.
(b) Double to quintuple mutations in TmXET6.3 (indicated in Table) influence hetero-transglycosylation activities. Activity values (%) with XG/[α(1-4)GalA*p*]$_5$ were calculated relative to those of the XG/XG-OS8 substrate pair. WT lacks activity. Standard deviations were calculated from three (n = 3) technical replicates.

alterations included involvements of additional positively charged lysine residues to those of K234 and K237 in TmXET6.3, demonstrating the importance of their location near R238. This finding is unsurprising as these mutations most likely increased, even more, the positive charge of the carboxyl-terminal region of the TmXET6.3 W75H/Y110R mutant. Nevertheless, the strongest effect on the suppression of activity with the XG/[α(1-4)GalA*p*]$_5$ substrate pair, was observed in W75H/Y110R/K234T/K237W, where the last two mutated residues are neutral or hydrophobic (Figure 4b). For the quadruple W75H/Y110R/K234T/Q241K and quintuple W75H/Y110R/K234T/K237W/S240K mutants, the activities with the XG/[α(1-4)GalA*p*]$_5$ pair decreased to values less than that in W75H/Y110R, as the inclusion of Q241K and S240K was suppressed by removing lysine residues in positions 234 and 237, in the first place. Hence, these observations confirmed the importance of K234 and K237 residues (alone or combined) in stabilising the binding of oppositely charged [α(1-4)GalA*p*]$_5$ in the acceptor binding site.

We also observed that the hetero-transglycosylation activities of the TmXET6.3 mutants with residues in positions corresponding to those of HvXET3 (W75H/Y110R/K234T/Q241K), and HvXET4 (W75H/Y110R/K234T) decreased in this order (Figure 4b), as shown experimentally in WT HvXET3 and HvXET4 isoforms (*cf.* Figure 5, Stratilová et al., 2020 therein). Here, the difference in activity was observed with the quintuple W75H/Y110R/K234T/K237W/S240K TmXET6.3 mutant (mutations equivalent to residues in HvXET6), which was comparable to that of W75H/Y110R/K234T (mutations equivalent to residues in HvXET4) (Figure 4b), although the activity of WT HvXET6 was significantly lower (*cf.* Figure 5, Stratilová et al., 2020 therein). This explanation could be justified by a modified electrostatic potential distribution of the W75H/Y110R mutant (Figure 5a) at the carboxyl-terminal region, due to the addition of the K234T/K237W/S240K mutations (Figure 5), a pattern, which is similar to that of WT HvXET6 (Figure 1c).

Molecular docking of the [α(1-4)GalA*p*]$_5$ acceptor in the binding site of the W75H/Y110R TmXET6.3 mutant,

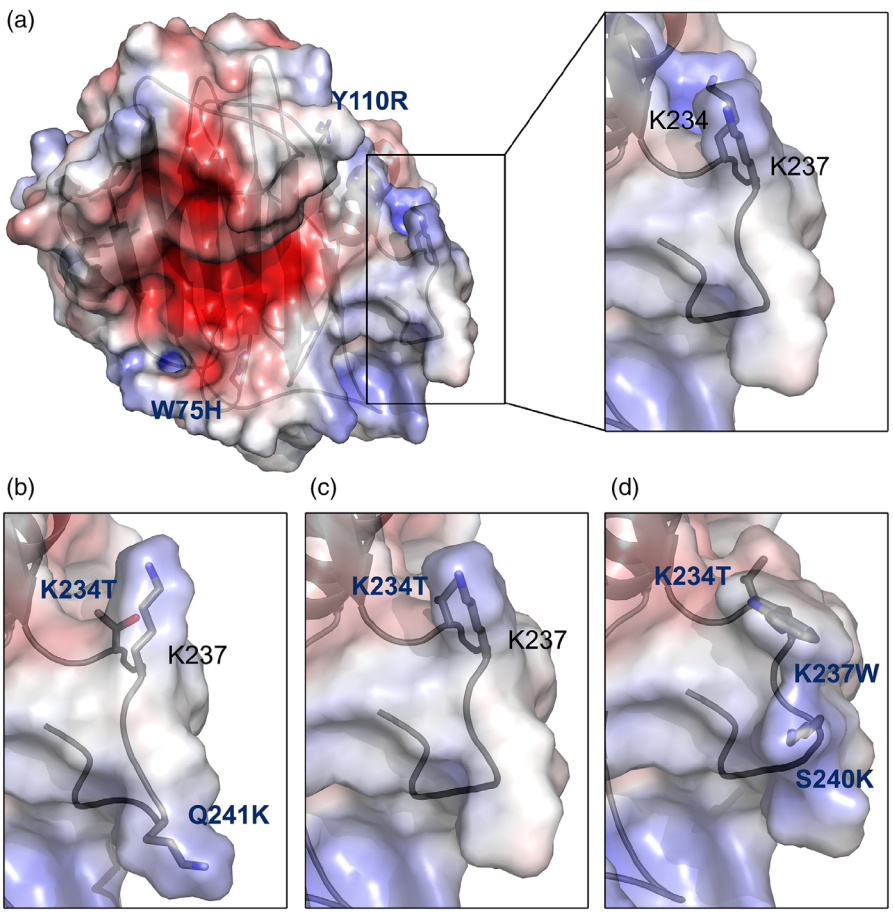

Figure 5. Surface morphologies of TmXET6.3 mutants coloured by electrostatic potentials (white, neutral; blue, +5 kT e^{-1}; red, −5 kT e^{-1}), in carboxyl-terminal regions of molecular models.
(a) W75H/Y110R double mutant; (b) W75H/Y110R/K234T/Q241K (mutations equivalent to residues in HvXET3); (c) W75H/Y110R/K234T (mutations equivalent to residues in HvXET4); (d) W75H/Y110R/K234T/K237W/S240K (mutations equivalent to residues in HvXET6).

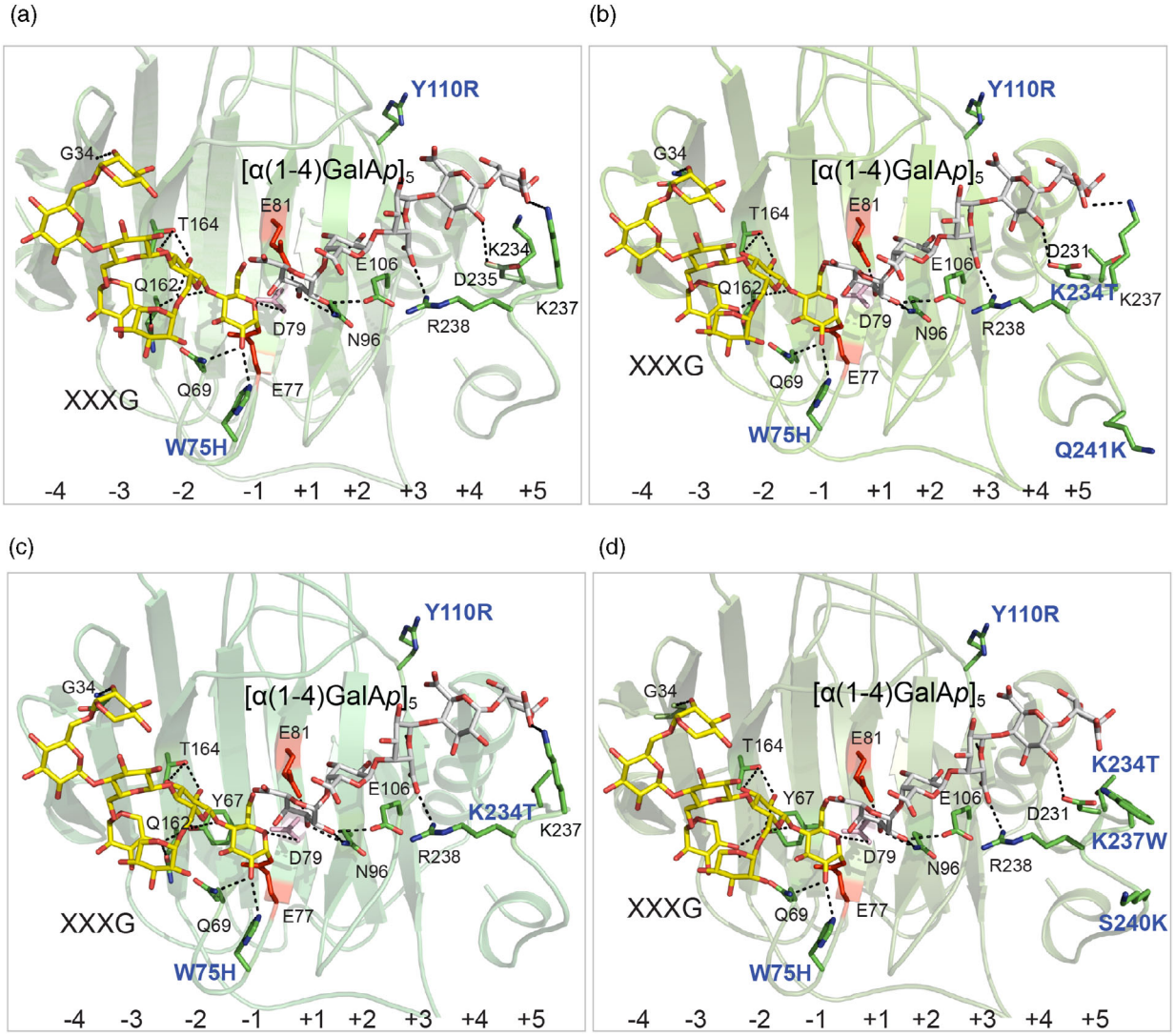

Figure 6. Molecular docking of the XXXG donor (yellow cpk sticks) and [α(1-4)GalA*p*]$_5$ acceptor (cpk sticks) substrates into 3D models of TmXET6.3 mutants. (a) W75H/Y110R; (b) W75H/Y110R/K234T/Q241K (mutations equivalent to residues HvXET3); (c) W75H/Y110R/K234T (mutations equivalent to residues HvXET4); (d) W75H/Y110R/K234T/K237W/S240K (mutations equivalent to residues HvXET6). The −4 to −1 subsites with XXXG and the +1 to +5 subsites with [α(1-4)GalA*p*]$_5$ in active sites are specified at the bottom of panels. Separations equal to or less than 4.0 Å of XXXG and [α(1-4)GalA*p*]$_5$ from residues are indicated.

with additional mutations of lysine residues (corresponding to lysine residue positions in the carboxyl-terminal regions of HvXET3, HvXET4, and HvXET6), demonstrated that [α(1-4)GalA*p*]$_5$ formed interactions only with K234, K237, and R238 at a distance of less than 4 Å (Figure 6). These interactions could be compared with those of the HvXET3, HvXET4, and HvXET6 isoforms (Figure S3). In the quintuple, TmXET6.3 W75H/Y110R/K234T/K237W/S240K mutant (corresponding to HvXET6, which lacks K237; Table 1), the K237W mutated residue, due to a larger side-chain forming a wide platform, made close contact with [α(1-4)GalA*p*]$_5$. Here, the interaction of the [α(1-4)GalA*p*]$_5$ acceptor with the lysine residue in position 240 (Figure 6d) was not observed in HvXET6 (Figure S3c). It could be suggested that these lysine residues and mutations thereof could influence an electrostatic potential of a larger part of the enzyme molecule, and therefore heterotransglycosylation activities in TmXET6.3 (Figure 6d). It is also evident from Figure S1, that the disposition of carboxyl-terminal K237 is relatively stable – those data signify that altered enzyme activities might stem from local changes of positive charges at and around surfaces of acceptor binding sites. To support these conclusions, the removal of carboxyl-terminal positively charged residues in TmXET6.3 led to an activity increase with Cello-OS acceptors (*cf.* Figure 8, Stratilová et al., 2019 therein), again pointing out, that these residues are not required for interactions with neutral acceptors. These and other factors (such as physical separations between key binding residues and acidic [α(1-4)GalA*p*]$_5$ that influence interactions

between acceptors and binding residues), could also result from the relatively balanced dispositions of carboxyl-terminal K237 (Figure S1), and R238 (Figure 6), and neighbouring residues, as demonstrated by MD simulations (Stratilová et al., 2022).

In an attempt to localise the hetero-transglycosylation XET activity in young germinated nasturtium seedlings *in situ* (Figure S4a), we separately dissected their epicotyls and roots, produced crude extracts, and incubated them with SR-labelled [α(1-4)GalA*p*]$_5$. After a 24-hour soaking of epicotyls and root extracts with fluorescently labelled [α(1-4)GalA*p*]$_5$, we imaged these plant extracts under a UV lamp (Figure S4b–e). Subsequently, we measured the activity of these crude extracts with the XG/SR-labelled [α(1-4)GalA*p*]$_5$ substrate pair, using size-exclusion HPLC (Figure S4f). We detected that while the fluorescence signal was absent in crude epicotyl extracts (Figure S4c), it was clearly discernible in root extracts, where it accumulated in root phloem/xylem components and CWs (Figure S4d), meaning that at least some proportion of [α(1-4)GalA*p*]$_5$ was incorporated in the CW polysaccharides of roots (Figure S4e), as previously observed in barley (Stratilová et al., 2020). This incorporation was further confirmed by determining the enzyme activity of root extracts by size-exclusion HPLC using the XG/ SR-labelled [α(1-4)GalA*p*]$_5$ substrate pair (Figure S4f).

Our observations indicate that the hetero-transglycosylation activity (with the XG/SR-labelled [α(1-4)GalA*p*]$_5$ substrate pair), was absent in epicotyl extracts, while it was found in root extracts (Figure S4f). This suggests that either the seed TmXET6.3 enzyme activity (Stratilová et al., 2019) was absent in epicotyls, although additional epicotyl isoforms present in the crude extract recognised the XG/XG-OS8 substrate pair (data not shown). In either case, it is likely that nasturtium seed, epicotyl, and root XETs might exhibit different substrate specificities or/and could be regulated differently at gene levels by corresponding transcription factors. These observations require further research and need to be examined in relation to the evolutionary history of nasturtium XET isoforms in various tissues, to uncover if these XET isoforms co-evolved, or were subjected to gene duplication and neo-functionalisation under selection pressures (Stratilová et al., 2020). Nevertheless, the possibility remains that in nasturtium and other plants, *XET* gene expression profiles differ during developmental stages, as shown in grapevine (Qiao et al., 2022), allowing for XET enzymes to perform precise functions in various cellular contexts (Folkendt et al., 2021).

In this work, we focussed on the engineering of substrate specificity of nasturtium TmXET6.3 through modifications of positively charged residues at the carboxyl terminus, to reveal new avenues to broaden their carbohydrate substrate recognition. We define, how this singularly carbohydrate-based enzymatic function of TmXET6.3 underlies linking diverse and complex carbohydrates that constitute plant CWs. We construe that broad substrate-specific XETs, such as TmXET6.3 could be further diversified to guarantee carbohydrate components heterogeneity, which is required for the generation of strong, yet flexible polysaccharide-based CWs. However, many questions regarding the roles of XETs in plant CW modification and re-modelling remain open – this work encourages those hypotheses that could offer new ideas and be applied to technological developments in the future.

CONCLUSIONS

Our findings demonstrate that the hetero-transglycosylation activity could be gained in the W75H/Y110R mutant and other mutants of TmXET6.3 with the XG/[α(1-4)GalA*p*]$_5$ substrate pair, that is, that this activity is directly affected by the configuration of its carboxyl-terminal acceptor binding site and consequently by the tertiary structure of an XET protein molecule. In addition to previously described roles of His75 and Arg110 residues in substrate binding, we revealed that Arg238 and Lys237, and a range of other lysine residues positioned in the carboxyl-terminal region of TmXE6.3, play key roles in donor and acceptor substrate binding. These data suggest that a broad acceptor specificity in TmXET6.3 could be diversified with respect to the chemical nature of an acceptor, and engineered by site-specific alterations of the acceptor binding site.

EXPERIMENTAL PROCEDURES

Mutants generation and plasmid construction

Point mutations were introduced in the truncated *XET6.3* gene starting at the Gly31 residue (numbering includes signal peptide). Mutations were introduced, using sequence-specific primers (Table S1) in the pJET1.2/blunt cloning vector (pJET-C'XET-W75H/Y110R) (Table S2) by the Quikchange Site-Directed Mutagenesis Kit (Agilent Technologies, Santa Clara, CA, USA), following the manufacturer protocol. The quintuple W75H/Y110R/K234T/K237W/S240K mutant was generated by introducing the S240K mutation into the pJET-W75H/Y110R/K234T/K237W-C'XET plasmid. Additional details are specified in Supporting Information.

Preparation of enzymes

Pichia pastoris strain GS115 (Invitrogen, Waltham, MA, USA) was used as a host for the over-expression of double W75H/Y110R, triple W75H/Y110R/K234T, W75H/Y110R/K237W, W75H/Y110R/S240K, and W75H/Y110R/Q241K, quadruple W75H/Y110R/K234T/K237W, and W75H/Y110R/K234T/K241Q, and quintuple W75H/Y110R/K234T/K237W/S240K mutants of TmXET6.3 as described previously (Stratilová et al., 2019, 2020). Additional details are specified in Supporting Information.

Substrates for enzyme reactions

The nasturtium seed XG (molecular mass >106 kDa), kindly donated by Dr Mayumi Shirakawa (Dainippon Pharmaceutical Co., Ltd., Osaka, Japan) served as a donor substrate and it was also used for the preparation of xyloglucan-derived oligosaccharides

(XG-OS). Other substrates included cellulose powder (fibres, medium) (Sigma–Aldrich, St. Louis, MO, USA) and pustulan [(1,6)-β-D-glucan] (Merck, Rahway, NJ, USA). Oligosaccharides (OS) derived from polysaccharides [XG-OS, cellotetraose (Cello-OS4), and pustulopentaose (Pu-OS5)] were prepared by the enzymic digestion of source polysaccharides (Kosík et al., 2010). The pentagalacturonic acid fragment [α(1-4)GalA*p*]$_5$ was a gift from Dr Anna Malovíková (Institute of Chemistry, Slovak Academy of Sciences, Slovakia). 3^3-α-L-Arabinofuranosyl-xylotetraose (AraXyl-OS), β(1–4,1-4,1-3)Glcp_4 (3^1-β-D-cellotriosyl-glucose), laminaripentaose (La-OS5) and xylopentaose (Xyl-OS5), were purchased from Neogen (Lansing, MI, USA). Abbreviations, descriptions, and chemical structures of all commercial and purified acceptor OS were defined previously (Stratilová et al., 2019, 2020) and are specified in Scheme S1. OSs were coupled with sulforhodamine (SR) as described (Kosík & Farkaš, 2008). The purity of SR-labelled OS acceptor substrates was confirmed by Ultraflex Bruker MALDI TOF/TOF spectrometry (Billerica, MA, USA), and thin-layer chromatography on silica gel plates (Merck) using the butan-1-ol:ethanol:water (5:3:2, by vol.) solvent system. The chromatograms were viewed under a UV lamp. The molar concentrations of labelled OS were calculated, based on the molar absorption coefficient for Lissamine rhodamine B sulphonyl chloride (Anaspec, Fremont, CA, USA), using ε566 = 85 000 M^{-1} cm^{-1}.

Enzyme activity assays

Enzyme activities were assayed by size-exclusion chromatography using a fluorimetric detection method, where the increase of fluorescence was monitored due to the incorporation of fluorescent SR-labelled acceptors into newly formed transglycosylation products through the catalytic action of XET enzymes. Reaction mixtures composed of donor substrates, XG, SR-labelled oligosaccharide acceptor substrates (Scheme S1), and enzyme preparations in 0.1 M ammonium acetate/glacial acetic acid buffer, pH 5.5, were in the volumetric ratio of 5:1:4; the final concentrations of donor and SR-labelled acceptors were 0.15% (w/v) and 27.5 μM, respectively. The mixtures were incubated at 25°C for various time intervals in vials placed in an autosampler of the high-performance liquid chromatography (HPLC) Dionex UltiMateTM 3000 device (Thermo Fischer Scientific, Waltham, MA, USA) and the Dionex UltiMateTM FLD-3100 fluorescence detector using an isocratic size-exclusion chromatography method. The analyses were performed on the TSKgel G3000 SWXL column, 7.8 mm × 300 mm (TosoHaas, Tokyo, Japan), eluted with 100 mM ammonium acetate/glacial acetic acid, pH 5.5 containing 20% (v/v) aqueous acetonitrile (φr = 0.2) at a flow-rate 0.5 ml min^{-1}. The detector was programmed using respective 530 nm and 575 nm excitation and emission wavelengths. The Chromeleon 6.80 software (Thermo Fischer Scientific) was used for device control and data acquisition. All assays were performed in triplicates (n = 3) and activities with standard deviations were calculated *via* Excel in Microsoft Office Professional 2016.

Comparative computational chemistry

Protein structural models were downloaded from the AlphaFold database (Jumper et al., 2021; Varadi et al., 2022) under the following accessions: TmXET6.3: AF-Q41614-F1; HvXET3: AF-P93671-F1; HvXET4: AF-P93672-F1 and HvXET6: AF-B1P1S7-F1. Protein structural models were prepared for docking using Protein Preparation Wizard (Schrödinger Release 2022: Protein Preparation Wizard). The coordinates of the donor XG hepta-oligosaccharide (XXXG or XG-OS7) donor were based on the position of the XG nona-oligosaccharide (XG-OS9 or XLLG) in the crystal structure of the TmNXG1-DYNIIG mutant complex (PDB 2vh9; Mark et al., 2009). The coordinates of the [α(1-4)GalA*p*]$_5$ acceptor were obtained using the tools available on the GLYCAM-web server [R.J. Woods Group (2005–XXXX) GLYCAM Web Complex Carbohydrate Research]. The [α(1-4)GalA*p*]$_5$ molecule was prepared for docking with LigPrep (Schrödinger Release 2022-3: LigPrep) and optimised using Jaguar (Bochevarov et al., 2013; Schrödinger Release 2022-4: Jaguar), and the DFT B3LYP-D3 method, including the 6-31G** basis set. The acceptor molecule was docked in optimised structures using the inner box size of 14 Å × 14 Å × 14 Å (corresponding to a total box size of 30 Å × 30 Å × 30 Å), and the Extra Precision protocol (Friesner et al., 2006; Glide version 6.7). Structural graphics images were generated using PyMol v.2.5.4 (Schrődinger LLC, Portland, OR, USA), and biomolecular electrostatics or electrostatic potentials were calculated through the plugin with the Adaptive Poisson-Boltzmann Solver (Jurrus et al., 2018) embedded in PyMol.

UniprotKB accessions

GH16_20 subfamily: TmXET6;3 – V5ZEF7; HvXET3 – P93671; HvXET4 – P93671; HvXET5 – P93668; HvXET6 – B1P1S7 or F2DM52; PttXET16A – Q8GZD5; GH16_21 subfamily (1,3;1,4)-β-D-glucan 4-glucanohydrolase – P27051.

ACKNOWLEDGEMENTS

This work was supported by the Operational Program Integrated Infrastructure of "Integration of multi-omics study results and biotechnological production of biologically important substances" project (ITMS 313011T560), co-financed by the European Regional Development Fund. B.S., S.Š., E.S., K.V. and S.K. appreciate the support from VEGA (Slovakia) (2/0137/20). M.H. acknowledges the funding from the Australian Research Council (DP120100900), the University of Adelaide (Australia), and the Huaiyin Normal University (China). Open access publishing facilitated by The University of Adelaide, as part of the Wiley - The University of Adelaide agreement via the Council of Australian University Librarians.

AUTHOR CONTRIBUTIONS

SŠ constructed plasmids and mutants. BS, ES and KV performed biochemical characterisations. BS and SK built 3D molecular models and docked ligands. BS and MH generated structural graphics. MH conducted bioinformatics analyses. ES and MH conceived and wrote the manuscript. All co-authors reviewed and approved the manuscript.

CONFLICT OF INTEREST

The authors declare they do not have any conflicts of interest.

DATA AVAILABILITY STATEMENT

All data can be found within the manuscript and its Supporting Information. Sequences of XET enzymes are available in GenBank under the accessions: TmXET6.3 (HF968473), HvXET3 (X93174), HvXET4 (X93175), HvXET5 (X91659) and HvXET6 (EU247793).

SUPPORTING INFORMATION

Additional Supporting Information may be found in the online version of this article.

Table S1. List of sequence-specific primers used to construct triple to quintuple mutants from TmXET6.3 W75H/Y110R for heterologous expression in *P. pastoris*.

Table S2. Plasmids that were used for the generation of TmXET6.3 mutants.

Scheme S1. Abbreviations, descriptions, and chemical structures of substrates used in this work.

Figure S1. Superpositions of TmXET6.3 at 0 ns (light green), and after 500 ns (green), and 1000 ns (dark green) MD simulation runs, focused on the position of K237 (box). RMSD values of superpositions between 0 and 500 ns, and 0 and 1000 ns are 1.7 Å and 2.1 Å, respectively.

Figure S2. Surface morphologies of binding sites of WT TmXET6.3 (left) and in W75H/Y110R (right) models, with electrostatic potentials (white, neutral; blue, +5 kT e^{-1}; red, −5 kT e^{-1}). Squares near W75/Y110 and W75H/Y110R residues point to differences in distributions of electrostatic potentials.

Figure S3. 3D models of (a) HvXET3 (green), (b) HvXET4 (cyan), and (c) HvXET6 (orange) in complex with the XXXG donor (yellow cpk sticks)/[α(1-4)GalA*p*]$_5$ acceptor (cpk sticks) substrate pair. Separations of 2.6–3.6 Å between interacting residues (cpk sticks) and XXXG in the −4 to −1 subsites, and [α(1-4)GalA*p*]$_5$ in the +1 to +5 subsites, are indicated in dashed lines. The −4 to +5 subsites are indicated at the bottom of the panels. Residues subjected to mutagenesis in this work are shown in bold blue types. Panels (a) and (b) are based on Stratilová et al. (2020).

Figure S4. A germinated nasturtium seedling under day-light (a), and (b) after incubation with the solution of fluorescently labelled [α(1-4)GalA*p*]$_5$ viewed under UV light. The in vivo incorporation of [α(1-4)GalA*p*]$_5$ into an epicotyl (c) and a root (d), with detail of CWs, shown in a root cross-section (e). The activity assay of crude extract from roots was detected by size-exclusion HPLC with the corresponding activity curve shown (f).

Video S1. Visualisation of the dynamics of the XXXG/neutral manno-tetra-oligosaccharide substrate pair binding by TmXET6.3 (broad specific) and PttXET16A (specific), obtained by MD simulation. The visualisation of the MD trajectory of the XXXG donor and manno-tetra-oligosaccharide acceptor substrates of both enzymes reveals the instability of the acceptor in specific PttXET16A. After 20 ns the manno-tetra-oligosaccharide acceptor changes its position in PttXET16A and approaches the carboxyl-terminal, which is unfavourable for glycosidic bond formation. Conversely, the manno-tetra-oligosaccharide acceptor in TmXET6.3 remains stable during the duration of the MD simulation and could lead to a hetero-transglycosylation reaction.

REFERENCES

Akdemir, K.H., **Seven, M.**, **Derman, Ü.C.** & **Harvey, A.J.** (2022) In silico analysis of XTH gene family from barley (*Hordeum vulgare* L.) and their comparative expression analysis during germination. *Turkish Journal of Botany*, **46**, 1.

Baran, R., **Sulová, Z.**, **Stratilová, E.** & **Farkaš, V.** (2000) Ping-pong character of nasturtium-seed xyloglucan endotransglycosylase (XET) reaction. *General Physiology and Biophysics*, **19**, 427–440.

Baumann, M.J., **Eklöf, J.M.**, **Michel, G.**, **Kallas, A.M.**, **Teeri, T.T.**, **Czjzek, M.** ***et al.*** (2007) Structural evidence for the evolution of xyloglucanase activity from xyloglucan endo-transglycosylases: biological implications for cell wall metabolism. *Plant Cell*, **19**, 1947–1963.

Behar, H., **Graham, S.W.** & **Brumer, H.** (2018) Comprehensive cross-genome survey and phylogeny of glycoside hydrolase family 16 members reveals the evolutionary origin of EG 16 and XTH proteins in plant lineages. *The Plant Journal*, **95**, 1114–1128.

Bochevarov, A.D., **Harder, E.**, **Hughes, T.F.**, **Greenwood, J.R.**, **Braden, D.A.**, **Philipp, D.M.** ***et al.*** (2013) Jaguar: A high-performance quantum chemistry software program with strengths in life and materials sciences. *International Journal of Quantum Chemistry*, **113**, 2110–2142.

Boerjan, W., **Ralph, J.** & **Baucher, M.** (2003) Lignin biosynthesis. *Annual Review of Plant Biology*, **54**, 519–546.

Burton, R.A., **Gidley, M.J.** & **Fincher, G.B.** (2010) Heterogeneity in the chemistry, structure and function of plant cell walls. *Nature Chemical Biology*, **6**, 724–732.

Cavalier, D.M. & **Keegstra, K.** (2006) Two xyloglucan xylosyltransferases catalyze the addition of multiple xylosyl residues to cellohexaose. *The Journal of Biological Chemistry*, **281**, 34197–34207.

Cavalier, D.M., **Lerouxel, O.**, **Neumetzler, L.**, **Yamauchi, K.**, **Reinecke, A.**, **Freshour, G.** ***et al.*** (2008) Disrupting two *Arabidopsis thaliana* xylosyltransferase genes results in plants deficient in xyloglucan, a major primary cell wall component. *Plant Cell*, **20**, 1519–1537.

Cocuron, J.C., **Lerouxel, O.**, **Drakakaki, G.**, **Alonso, A.P.**, **Liepman, A.H.**, **Keegstra, K.** ***et al.*** (2007) A gene from the cellulose synthase-like C family encodes a β-1,4 glucan synthase. *Proceedings of the National Academy of Sciences of the United States of America*, **104**, 8550–8555.

Cosgrove, D.J. (2005) Growth of the plant cell wall. *Nature Reviews. Molecular Cell Biology*, **6**, 850–861.

Cosgrove, D.J. (2015) Plant cell wall extensibility: connecting plant cell growth with cell wall structure, mechanics, and the action of wall modifying enzymes. *Journal of Experimental Botany*, **67**, 463–476.

Culbertson, A.T., **Chou, Y.H.**, **Smith, A.L.**, **Young, Z.T.**, **Tietze, A.A.**, **Cottaz, S.** ***et al.*** (2016) Enzymatic activity of xyloglucan xylosyltransferase 5. *Plant Physiology*, **171**, 1893–1904.

Déjardin, A., **Laurans, F.**, **Arnaud, D.**, **Breton, C.**, **Pilate, G.** & **Leplé, J.-C.** (2010) Wood formation in angiosperms. *Comptes Rendus Biologies*, **333**, 325–334.

Drula, E., **Garron, M.-L.**, **Dogan, S.**, **Lombard, V.**, **Henrisatt, B.** & **Terrapon, N.** (2022) The carbohydrate-active enzyme database: functions and literature. *Nucleic Acids Research*, **50**, D571–D577.

Eklöf, J.M. & **Brumer, H.** (2010) The XTH gene family: an update on enzyme structure, function, and phylogeny in xyloglucan remodeling. *Plant Physiology*, **153**, 456–466.

Eklöf, J.M., **Shojania, S.**, **Okon, M.**, **McIntosh, L.P.** & **Brumer, H.** (2013) Structure–function analysis of a broad specificity Populus trichocarpa endo-β-glucanase reveals an evolutionary link between bacterial licheninases and plant XTH gene products. *The Journal of Biological Chemistry*, **288**, 15786–15799.

Faik, A., **Price, N.J.**, **Raikhel, N.V.** & **Keegstra, K.** (2002) An *Arabidopsis* gene encoding an alpha-xylosyltransferase involved in xyloglucan biosynthesis. *Proceedings of the National Academy of Sciences of the United States of America*, **99**, 7797–7802.

Fangel, J., **Ulvskov, P.**, **Knox, J.P.**, **Mikkelsen, M.**, **Harholt, J.**, **Popper, Z.** ***et al.*** (2012) Cell wall evolution and diversity. *Frontiers in Plant Science*, **3**, 153.

Farrokhi, N., **Burton, R.A.**, **Brownfield, L.**, **Hrmova, M.**, **Wilson, S.M.**, **Bacic, A.** ***et al.*** (2009) Plant cell wall biosynthesis: genetic, biochemical and functional genomics approaches to the identification of key genes. *Plant Biotechnology Journal*, **4**, 145–167.

Fincher, G.B. (2009) Revolutionary times in our understanding of cell wall biosynthesis and remodeling in the grasses. *Plant Physiology*, **149**, 7–37.

Folkendt, L., **Lohmann, I.** & **Domsch, K.** (2021) An evolutionary perspective on Hox binding site preferences in two different tissues. *Journal of Developmental Biology*, **9**, 57.

Franková, L. & **Fry, S.C.** (2013) Biochemistry and physiological roles of enzymes that 'cut and paste' plant cell-wall polysaccharides. *Journal of Experimental Botany*, **64**, 3519–3550.

Friesner, R.A., **Murphy, R.B.**, **Repasky, M.P.**, **Frye, L.L.**, **Greenwood, J.R.**, **Halgren, T.A.** ***et al.*** (2006) Extra precision glide: docking and scoring incorporating a model of hydrophobic enclosure for protein-ligand complexes. *Journal of Medicinal Chemistry*, **49**, 6177–6196.

Fry, S.C. (2004) Primary cell wall metabolism: tracking the careers of wall polymers in living plant cells. *The New Phytologist*, **161**, 641–675.

Fry, S.C., **Franková, L.** & **Chormova, D.** (2011) Setting the boundaries: primary cell wall synthesis and expansion. *The Biochemist*, **33**, 14–19.

Gille, S., **de Souza, A.**, **Xiong, G.**, **Benz, M.**, **Cheng, K.**, **Schultink, A.** ***et al.*** (2011) O-acetylation of *Arabidopsis* hemicellulose xyloglucan requires

AXY4 or AXY4L, proteins with a TBL and DUF231 domain. *Plant Cell*, **23**, 4041–4053.

Glide. (2015) *Glide, version 6.7*. New York, NY: Schrödinger, LLC.

Hahn, M., **Pons, J.**, **Planas, A.**, **Querol, E.** & **Heinemann, U.** (1995) Crystal structure of bacillus licheniformis 1,3-1,4-beta-D-glucan 4-glucanohydrolase at 1.8 Å resolution. *FEBS Letters*, **374**, 221–224.

Hayashi, T. (1989) Xyloglucans in the primary cell wall. *Annual Review of Plant Physiology and Plant Molecular Biology*, **40**, 139–168.

Holland, C., **Simmons, T.J.**, **Meulewaeter, F.**, **Hudson, A.** & **Fry, S.C.** (2020) Three highly acidic equisetum XTHs differ from hetero-trans-β-glucanase in donor substrate specificity and are predominantly xyloglucan homotransglucosylases. *Journal of Plant Physiology*, **251**, 153210.

Hrmova, M., **Farkas, V.**, **Harvey, A.J.**, **Lahnstein, J.**, **Wischmann, B.**, **Kaewthai, N.** ***et al.*** (2009) Substrate specificity and catalytic mechanism of a xyloglucan xyloglucosyl transferase HvXET6 from barley (*Hordeum vulgare* L.). *The FEBS Journal*, **276**, 437–456.

Hrmova, M., **Farkaš, V.**, **Lahnstein, J.** & **Fincher, G.B.** (2007) A barley xyloglucan xyloglucosyl transferase covalently links xyloglucan, cellulosic substrates, and (1,3;1,4)-β-D-glucans. *The Journal of Biological Chemistry*, **283**, 27344.

Hrmova, M., **MacGregor, E.A.**, **Biely, P.**, **Stewart, R.J.** & **Fincher, G.B.** (1998) Substrate binding and catalytic mechanism of a barley β-D-glucosidase/(1,4)-β-D-glucan exohydrolase. *The Journal of Biological Chemistry*, **273**, 11134–11143.

Hrmova, M., **Stratilová, B.** & **Stratilová, E.** (2022) Broad specific xyloglucan: xyloglucosyl transferases are formidable players in the re-modelling of plant cell wall structures. *International Journal of Molecular Sciences*, **23**, 1656.

Iraki, N.M., **Bressan, R.A.**, **Hasegawa, P.M.** & **Carpita, N.C.** (1989) Alteration of the physical and chemical structure of the primary cell wall of growth-limited plant cells adapted to osmotic stress. *Plant Physiology*, **91**, 39–47.

Jensen, J.K., **Schultink, A.**, **Keegstra, K.**, **Wilkerson, C.G.** & **Pauly, M.** (2012) RNA-seq analysis of developing nasturtium seeds (*Tropaeolum majus*): identification and characterization of an additional galactosyltransferase involved in xyloglucan biosynthesis. *Molecular Plant*, **5**, 984–992.

Johansson, P., **Brumer, H., 3rd**, **Baumann, M.J.**, **Kallas, A.M.**, **Henriksson, H.**, **Denman, S.E.** ***et al.*** (2004) Crystal structures of a poplar xyloglucan endotransglycosylase reveal details of transglycosylation acceptor binding. *Plant Cell*, **16**, 874–886.

Jumper, J., **Evans, R.**, **Pritzel, A.**, **Green, T.**, **Figurnov, M.**, **Ronneberger, O.** ***et al.*** (2021) Highly accurate protein structure prediction with AlphaFold. *Nature*, **596**, 583–589.

Jurrus, E., **Engel, D.**, **Star, K.**, **Monson, K.**, **Brandi, J.**, **Felberg, L.E.** ***et al.*** (2018) Improvements to the APBS biomolecular solvation software suite. *Protein Science*, **27**, 112–128.

Kaewthai, N., **Gendre, D.**, **Eklöf, J.M.**, **Ibatullin, F.M.**, **Ezcurra, I.**, **Bhalerao, R.P.** ***et al.*** (2013) Group III-A XTH genes of Arabidopsis encode predominant xyloglucan endohydrolases that are dispensable for normal growth. *Plant Physiology*, **161**, 440–454.

Keitel, T., **Simon, O.**, **Borriss, R.** & **Heinemann, U.** (1993) Molecular and active-site structure of a bacillus 1,3–1,4-β-glucanase. *Proceedings of the National Academy of Sciences of the United States of America*, **90**, 5287–5291.

Kim, S.-J., **Chandrasekar, B.**, **Rea, A.**, **Danhof, L.**, **Zemelis-Durfee, S.**, **Thrower, N.** ***et al.*** (2020) The synthesis of xyloglucan, an abundant plant cell wall polysaccharide, requires CSLC function. *Proceedings of the National Academy of Sciences of the United States of America*, **117**, 20316–20324.

Kosík, O., **Auburn, R.P.**, **Russell, S.**, **Stratilová, E.**, **Garajová, S.**, **Hrmova, M.** ***et al.*** (2010) Polysaccharide microarrays for high-throughput screening of transglycosylase activities in plant extracts. *Glycoconjugate Journal*, **27**, 79–87.

Kosík, O. & **Farkaš, V.** (2008) One-pot synthesis of xyloglucan oligosaccharides fluorescently labeled with sulforhodamine. *Analytical Biochemistry*, **375**, 232–236.

Kozlova, L.V., **Nazipova, A.R.**, **Gorshkov, O.V.**, **Petrova, A.A.** & **Gorshkova, T.A.** (2020) Elongating maize root: zone-specific combinations of polysaccharides from type I and tape II primary cell walls. *Scientific Reports*, **10**, 10956.

Kushwah, S., **Banasiak, A.**, **Nishikubo, N.**, **Derba-Maceluch, M.**, **Majda, M.**, **Endo, S.** ***et al.*** (2020) *Arabidopsis* XTH4 and XTH9 contribute to wood cell expansion and secondary wall formation. *Plant Physiology*, **182**, 1946–1965.

Kutsuno, T., **Chowhan, S.**, **Kotake, T.** & **Takahashi, D.** (2023) Temporal cell wall changes during cold acclimation and deacclimation and their potential involvement in freezing tolerance and growth. *Physiologia Plantarum*, **175**, e13837.

Liu, L., **Hsia, M.M.**, **Dama, M.**, **Vogel, J.** & **Pauly, M.** (2016) A xyloglucan backbone 6-O-acetyltransferase from *Brachypodium distachyon* modulates xyloglucan xylosylation. *Molecular Plant*, **9**, 615–617.

Madson, M., **Dunand, C.**, **Li, X.**, **Verma, R.**, **Vanzin, G.F.**, **Caplan, J.** ***et al.*** (2003) The MUR3 gene of *Arabidopsis* encodes a xyloglucan galactosyltransferase that is evolutionarily related to animal exostosins. *Plant Cell*, **15**, 1662–1670.

Marcus, S.E., **Verhertbruggen, Y.**, **Hervé, C.**, **Ordaz-Ortiz, J.J.**, **Farkas, V.**, **Pedersen, H.L.** ***et al.*** (2008) Pectic homogalacturonan masks abundant sets of xyloglucan epitopes in plant cell walls. *BMC Plant Biology*, **8**, 60.

Mark, P., **Baumann, M.J.**, **Eklöf, J.M.**, **Gullfot, F.**, **Michel, G.**, **Kallas, A.M.** ***et al.*** (2009) Analysis of nasturtium TmNXG1 complexes by crystallography and molecular dynamics provides detailed insight into substrate recognition by family GH16 xyloglucan endo-transglycosylases and endohydrolases. *Proteins*, **75**, 820–836.

McCann, M.C. & **Knox, J.P.** (2011) Plant cell wall biology: polysaccharides in architectural and developmental contexts. *Annual Review of Plant Biology*, **41**, 343–366.

McGregor, N., **Yin, V.**, **Tung, C.-C.**, **Van Petegem, F.** & **Brumer, H.** (2017) Crystallographic insight into the evolutionary origins of xyloglucan endotransglycosylases and endohydrolases. *The Plant Journal*, **89**, 651–670.

Mnich, E., **Bjarnholt, N.**, **Eudes, A.**, **Harholt, J.**, **Holland, C.**, **Jørgensen, B.** ***et al.*** (2020) Phenolic cross-links: building and de-constructing the plant cell wall. *Natural Product Reports*, **37**, 919–961.

Ochoa-Meza, L.C., **Quintana-Obregón, E.A.**, **Vargas-Arispuro, I.**, **Falcón-Rodríguez, A.B.**, **Aispuro-Hernández, E.**, **Virgen-Ortiz, J.J.** ***et al.*** (2021) Oligosaccharins as elicitors of defense responses in wheat. *Polymers (Basel)*, **13**, 3105.

Pauly, M. & **Keegstra, K.** (2016) Biosynthesis of the plant cell wall matrix polysaccharide xyloglucan. *Annual Review of Plant Biology*, **67**, 235–259.

Pei, D.S., **Sun, Y.H.**, **Chen, C.H.**, **Chen, S.P.**, **Wang, Y.P.**, **Hu, W.** ***et al.*** (2008) Identification and characterization of a novel gene differentially expressed in zebrafish cross-subfamily cloned embryos. *BMC Developmental Biology*, **8**, 29.

Peña, M.J., **Darvill, A.G.**, **Eberhard, S.**, **York, W.S.** & **O'Neill, M.A.** (2008) Moss and liverwort xyloglucans contain galacturonic acid and are structurally distinct from the xyloglucans synthesized by hornworts and vascular plants. *Glycobiology*, **18**, 891–904.

Peña, M.J., **Kong, Y.**, **York, W.S.** & **O'Neill, M.A.** (2012) A galacturonic acid-containing xyloglucan is involved in *Arabidopsis* root hair tip growth. *Plant Cell*, **24**, 4511–4524.

Perrin, R.M., **DeRocher, A.E.**, **Bar-Peled, M.**, **Zeng, W.**, **Norambuena, L.**, **Orellana, A.** ***et al.*** (1999) Xyloglucan fucosyltransferase, an enzyme involved in plant cell wall biosynthesis. *Science*, **284**, 1976–1979.

Popper, Z.A. & **Fry, S.C.** (2003) Primary cell wall composition of bryophytes and charophytes. *Annals of Botany*, **91**, 1–12.

Popper, Z.A. & **Fry, S.C.** (2004) Primary cell wall composition of the pteridophytes and spermatophytes. *The New Phytologist*, **164**, 165–174.

Popper, Z.A. & **Fry, S.C.** (2005) Widespread occurrence of a covalent linkage between xyloglucan and acidic polysaccharides in suspension-cultured angiosperm cells. *Annals of Botany*, **96**, 91–99.

Popper, Z.A., **Michel, G.**, **Hervé, C.**, **Domozych, D.S.**, **Willats, W.G.**, **Tuohy, M.G.** ***et al.*** (2011) Evolution and diversity of plant cell walls: from algae to flowering plants. *Annual Review of Plant Biology*, **62**, 567–590.

Qiao, T., **Zhang, L.**, **Yu, Y.**, **Pang, Y.**, **Tang, X.**, **Wang, X.** ***et al.*** (2022) Identification and expression analysis of xyloglucan endotransglucosylase/hydrolase (XTH) family in grapevine (*Vitis vinifera* L.). *PeerJ*, **10**, e13546.

R.J. Woods Group. (2005–XXXX) *GLYCAM Web Complex Carbohydrate Research Center*. Athens, GA, USA: University of Georgia [accessed on 17 July 2022].

Rose, J.K., **Braam, J.**, **Fry, S.C.** & **Nishitani, K.** (2002) The XTH family of enzymes involved in xyloglucan endotransglucosylation and endohydrolysis: current perspectives and a new unifying nomenclature. *Plant & Cell Physiology*, **43**, 1421–1435.

Saura-Valls, M., **Fauré, R.**, **Ragàs, S.**, **Piens, K.**, **Brumer, H.**, **Teeri, T.T.** ***et al.*** (2006) Kinetic analysis using low-molecular mass xyloglucan oligosaccharides defines the catalytic mechanism of a *Populus* xyloglucan endotransglycosylase. *The Biochemical Journal*, **395**, 99–106.

Scheller, H.V. & **Ulvskov, P.** (2010) Hemicelluloses. *Annual Review of Plant Biology*, **61**, 263–289.

Schrödinger Release 2022-2. (2015) *Schrödinger Release 2022-2: Protein Preparation Wizard; Epik*. New York, NY: Schrödinger, LLC.

Schrödinger Release 2022-3. (2021) *Schrödinger Release 2022-3: LigPrep*. New York, NY: Schrödinger, LLC.

Schrödinger Release 2022-4. (2021) *Schrödinger Release 2022-4: Jaguar*. New York, NY: Schrödinger, LLC.

Seven, M., **Derman, C.** & **Harvey, A.** (2021) Enzymatic characterization of ancestral/group-IV clade xyloglucan endotransglycosylase/hydrolase enzymes reveals broad substrate specificities. *The Plant Journal*, **106**, 1660–1673.

Shinohara, N. & **Nishitani, K.** (2021) Cryogenian origin and subsequent diversification of the plant cell-wall enzyme XTH family. *Plant & Cell Physiology*, **62**, 874–1889.

Shinohara, N., **Sunagawa, N.**, **Tamura, S.**, **Yokoyama, R.**, **Ueda, M.**, **Igarashi, K.** ***et al.*** (2017) The plant cell-wall enzyme AtXTH3catalyses covalent cross-linking between cellulose and cello-oligosaccharide. *Scientific Reports*, **7**, 46099.

Simmons, T.J., **Mohler, K.E.**, **Holland, C.**, **Goubet, F.**, **Franková, L.**, **Houston, D.R.** ***et al.*** (2015) Hetero-trans-β-glucanase, an enzyme unique to *Equisetum* plants, functionalizes cellulose. *The Plant Journal*, **83**, 753–769.

Sørensen, I., **Domozych, D.** & **Willats, W.G.T.** (2010) How have plant cell walls evolved? *Plant Physiology*, **153**, 366–372.

Stratilová, B., **Firáková, Z.**, **Klaudiny, J.**, **Šesták, S.**, **Kozmon, S.**, **Strouhalová, D.** ***et al.*** (2019) Engineering the acceptor substrate specificity in the xyloglucan endotransglycosylase TmXET6.3 from nasturtium seeds (Tropaeolum majus L.). *Plant Molecular Biology*, **100**, 181–197.

Stratilová, B., **Šesták, S.**, **Mravec, J.**, **Garajová, S.**, **Pakanová, Z.**, **Vadinová, K.** ***et al.*** (2020) Another building block in the plant cell wall: barley xyloglucan xyloglucosyl transferases link covalently xyloglucan and anionic oligosaccharides derived from pectin. *The Plant Journal*, **104**, 752–767.

Stratilová, B., **Stratilová, E.**, **Hrmova, M.** & **Kozmon, S.** (2022) Definition of the acceptor substrate binding specificity in plant xyloglucan endotransglycosylases using computational chemistry. *International Journal of Molecular Sciences*, **23**, 11838.

Thompson, J.E., **Smith, R.C.** & **Fry, S.C.** (1997) Xyloglucan undergoes interpolymeric transglycosylation during binding to the plant cell wall in vivo: evidence from 13C/3H dual labelling and isopycnic centrifugation in caesium trifluoroacetate. *The Biochemical Journal*, **327**, 699–708.

Vanzin, G.F., **Madson, M.**, **Carpita, N.C.**, **Raikhel, N.V.**, **Keegstra, K.** & **Reiter, W.-D.** (2002) The mur2 mutant of *Arabidopsis thaliana* lacks fucosylated xyloglucan because of a lesion in fucosyltransferase AtFUT1. *Proceedings of the National Academy of Sciences of the United States of America*, **99**, 3340–3345.

Varadi, M., **Anyango, S.**, **Deshpande, M.**, **Nair, S.**, **Natassia, C.**, **Yordanova, G.** ***et al.*** (2022) AlphaFold protein structure database: massively expanding the structural coverage of protein-sequence space with high-accuracy models. *Nucleic Acids Research*, **50**, D439–D444.

Viborg, A.H., **Terrapon, N.**, **Lombard, V.**, **Michel, G.**, **Czjzek, M.**, **Henrissat, B.** ***et al.*** (2019) A subfamily roadmap for functional glycogenomics of the evolutionarily diverse glycoside hydrolase family 16 (GH16). *The Journal of Biological Chemistry*, **294**, 15973–15986.

Vuttipongchaikij, S., **Brocklehurst, D.**, **Steele-King, C.**, **Ashford, D.A.**, **Gomez, L.D.** & **McQueen-Mason, S.J.** (2012) *Arabidopsis* GT34 family contains five xyloglucan α-1,6-xylosyltransferases. *The New Phytologist*, **195**, 585–595.

Weng, J.K. & **Chapple, C.** (2010) The origin and evolution of lignin biosynthesis. *The New Phytologist*, **187**, 273–285.

York, W.S., **Van Halbeek, H.**, **Darvill, A.G.** & **Albersheim, P.** (1990) Structural analysis of xyloglucan oligosaccharides by 1H-n.m.r. spectroscopy and fast-atom-bombardment mass spectrometry. *Carbohydrate Research*, **200**, 9–31.

Zabotina, O.A., **Avci, U.**, **Cavalier, D.**, **Pattathil, S.**, **Chou, Y.H.**, **Eberhard, S.** ***et al.*** (2012) Mutations in multiple XXT genes of Arabidopsis reveal the complexity of xyloglucan biosynthesis. *Plant Physiology*, **159**, 1367–1384.

Zabotina, O.A., **van de Ven, W.T.**, **Freshour, G.**, **Drakakaki, G.**, **Cavalier, D.**, **Mouille, G.** ***et al.*** (2008) *Arabidopsis* XXT5 gene encodes a putative alpha-1,6-xylosyltransferase that is involved in xyloglucan biosynthesis. *The Plant Journal*, **56**, 101–115.

Zhong, R., **Cui, D.**, **Phillips, D.R.**, **Richardson, E.A.** & **Ye, Z.H.** (2020) A group of O-acetyltransferases catalyze xyloglucan backbone acetylation and can alter xyloglucan xylosylation pattern and plant growth when expressed in *Arabidopsis*. *Plant & Cell Physiology*, **61**, 1064–1079.

Zhong, R., **Cui, D.** & **Ye, Z.H.** (2017) Regiospecific acetylation of xylan is mediated by a group of DUF231-containing O-acetyltransferases. *Plant & Cell Physiology*, **58**, 2126–2138.

Zhong, R., **Cui, D.** & **Ye, Z.H.** (2018) Xyloglucan O-acetyltransferases from *Arabidopsis thaliana* and *Populus trichocarpa* catalyze acetylation of fucosylated galactose residues on xyloglucan side chains. *Planta*, **248**, 1159–1171.